Influence of quantum dot morphology on the optical properties of GaSb/GaAs multilayers

C. Greenhill,[1] A.S. Chang,[1,3] E. Zech,[1] S. Clark,[2] G. Balakrishnan,[2] R. S. Goldman[1*]

[1]*Department of Materials Science and Engineering, University of Michigan, Ann Arbor, Michigan, 48109, USA*

[2]*Department of Electrical and Computer Engineering, University of New Mexico, Albuquerque, New Mexico, 87106, USA*

[3]*Department of Materials Science and Engineering, Northwestern University, Evanston, Illinois, 60208, USA*

May 30, 2020

Abstract

We examine the influence of quantum dot (QD) morphology on the optical properties of two dimensional (2D) GaSb/GaAs multilayers, with and without 3D nanostructures. Using nanostructure sizes from scanning transmission electron microscopy (STEM) and local Sb compositions from local electrode atom probe (LEAP) tomography as input into self-consistent Schrödinger-Poisson simulations based on 8x8 **k·p** theory, we compute confinement energies for quantum dots (QDs), circular arrangements of smaller QDs, termed QD-rings, and 2D layers on GaAs substrates. The computed confinement energies and the measured photoluminescence emission energies increase from QDs to QD-rings to 2D layers, enabling direct association of nanostructure morphologies with the optical properties of the GaSb/GaAs multilayers. This work opens up opportunities for tailoring near to far infrared optoelectronic devices by varying the QD morphology.

*Corresponding author: rsgold@umich.edu

Due to the predicted strain and composition dependence of nested (type I) versus staggered (type II) band alignments,[1] GaSb/GaAs QDs are promising for a variety of optoelectronic applications, including solar-cells,[2] photodetectors,[3] charged-based memory[4,5] and light-emitters.[6] Typically, the nucleation of three-dimensional (3D) nanostructures from two-dimensional (2D) GaSb "wetting" layers shifts photoluminescence (PL) emissions further into the infrared range. In addition, within GaSb/GaAs multilayers, atomic structures ranging from QDs to quantum rings (QRs) and clusters have been observed.[7,8,9] However, the association of emission energies with specific nanostructure types (i.e. QDs vs. QRs vs. clusters) remains elusive. For example, PL energies at 0.92 eV[10], 1.01-1.05 eV[11], 1.1eV,[12,13] 1.13-1.18 eV,[14] and 1.2 eV[15] have been attributed to capped GaSb QDs with heights ranging from 6 to 10 nm, with no apparent correlation between QD size and emission energy. On the other hand, similar PL energies of 0.9-1.08 eV,[16] 0.95 eV,[17] 1.02 eV, and 1.06 eV[18] have been attributed to GaSb QRs. In some cases, multiple-peak emissions for GaSb QDs are attributed to bimodal size distributions.[19] Indeed, the nanoscale morphology is seldomly discussed in reports on multi-layered GaSb/GaAs devices. To date, there is a lack of consensus on the origins of various emission energies for GaSb/GaAs multilayers.

Here, we report on the morphology and optical properties of GaSb/GaAs multilayers, with and without 3D nanostructures. Using cross-sectional scanning transmission electron microscopy (XSTEM), local electrode atom-probe tomography (LEAP), and PL spectroscopy, in conjunction with Schrödinger-Poisson simulations based on 8x8 $\mathbf{k}\cdot\mathbf{p}$ theory, we identify the influences of nanostructure height and core composition on PL emissions. We associate emissions, in order of increasing energy to QDs; circular arrangements of smaller QDs, termed QD-rings (QDRs), and 2D layers (or wetting layers (WLs)). This work opens up opportunities for tailoring PL emission energies by varying QD morphology, as needed for optimizing near-to-far-infrared optoelectronic devices.

For these investigations, 5 periods of GaSb/GaAs multilayers consisting of alternating layers of GaSb (3 or 4 MLs) and 25 nm p-GaAs spacers were deposited on p-type GaAs (001) substrates by molecular-beam epitaxy using solid Ga, As_2, and Sb_2 sources, as described in supplementary materials. Following growth, thin foils for XSTEM were prepared using mechanical grinding to <20 μm, followed by argon-ion milling using a Gatan Precision Ion Polishing system.[20] Bright (BF) STEM was carried out at 300 kV using the JEOL 3100. For LEAP studies, conical-shaped specimens were prepared by a standard lift-out procedure and loaded into the Cameca LEAP 4000X, which was maintained at cryogenic temperatures (<25 K) under ultrahigh vacuum conditions (3.0×10^{-11} Torr), similar to earlier studies of GaAsSb.[21] LEAP experiments were performed in voltage-pulsing mode at 200 kHz with a 20% pulse fraction and constant detection rate of 37%. 3D reconstructions of LEAP datasets were performed using Cameca's Integrated Visualization and Analysis Software. PL measurements (T=20 K) were collected in a helium flow cryostat using a 250 μm slit, single channel InGaAs detector, and 10 mW HeNe laser operating at 633 nm. Finally, using nanostructures size and Sb composition gradients from STEM and LEAP, hole confinement energies in $GaAs_{1-x}Sb_x$/GaAs were calculated using nextnano.[22]

Large-scale XSTEM images of the 3ML and 4ML GaSb/GaAs superlattices, shown in Figs. 1(a) and 1(b), reveal isolated WLs and WLs with 3D nanostructures, respectively. Henceforth, we refer to the 3ML (4ML) superlattice as "2DLs" ("2DLs+3DNSs"). We note the presence of clustering in the first (bottom) GaSb layer, as indicated by yellow arrows in Fig. 1(b). Since the volume of deposited GaSb in each layer is constant, the 3D nanostructures in subsequent layers are likely due to enhanced island nucleation at strain energy minima above buried islands.[23]

Although dislocations are not apparent in the vicinity of the nanostructures, strain-induced Sb out-diffusion into the GaAs spacers may have occurred, as depicted by the black arrows in Fig. 1(b).

To identify and quantify the nanostructure types within 2DLs+3DNSs, we apply the following criteria. For GaSb QDs, as shown in Fig. 1(c), Sb atoms form a "lens" shape, similar to earlier studies of GaSb/GaAs and InAs/GaAs.[2,20] In addition, nanostructures with distinct lobes of Sb are apparent, as depicted by white dotted lines in Figs. 1(d) and 1(e). We denote nanostructures with two and three (or more) distinct Sb lobes as (d) QRs and (e) clusters, respectively. Due to their similar structures, the formation mechanisms of the QRs/clusters are expected to be similar.[7,9,24] Finally, the average heights for the QDs (QRs/clusters) are 7 ± 4 nm (4 ± 2 nm). In a region of ~200 μm^2, 114 GaSb nanostructures were observed, with 64% QDs, 17% QRs, and 18% clusters.

To determine Sb incorporation into the GaSb layers, we consider x-z views of LEAP reconstructions for 2DLs and 2DLs+3DNSs in Figs. 2(a) and 2(b), along with representative 1D profiles of the fraction of Sb atoms, x_{Sb}, in blue. Due to premature tip fracturing at ~7kV during the LEAP experiment, data for two (three) of the five layers were collected for 2DLs (2DLs+3DNSs). For 2DLs and 2DLs+3DNSs, the average x_{Sb} values are 0.08 and 0.12 within the 2D layers, with x_{Sb}< ~0.01 within the GaAs spacer regions.

To determine local x_{Sb}, we consider isosurfaces at various x_{Sb} thresholds. Fig. 3(a) shows the x_{Sb} > 0.20 isosurface of 2DLs, with x-y views of the top layer at x_{Sb} > 0.04, 0.08, 0.10 and 0.16 in Figs. 3(b), (c), (d), and (e), respectively. As the x_{Sb} threshold increases from 0.04 in Fig. 3(b) to 0.16 in Fig. 3(e), spatial variations in x_{Sb} are observed. For 2DLs, the maximum x_{Sb} is approximately 0.18, and 3D nanostructures are not apparent, consistent with the XSTEM images in Fig. 1(a).

For 2DLS+3DNS, the $x_{Sb} > 0.24$ isosurface is shown in Fig. 4(a), with x-y views of the top layer at $x_{Sb} > 0.24$ in Fig. 4(b) and the bottom layer at $x_{Sb} > 0.28$ in Fig. 4(c). Maximum core values of $x_{Sb} = 0.90$ (0.42) for a QD (QR) are presented in Fig. 4(b). It is interesting to note that as the x_{Sb} threshold increases from > 0.24 to 0.28, the apparent "QR" in the bottom layer of Fig. 4(a) consist of a circular arrangement of QDs with smaller Sb-rich cores as shown Fig. 4(c), which we term quantum dot ring (QDR). At the centers of the individual cores of the QDR, the maximum values of x_{Sb} are 0.36, 0.38, 0.40, and 0.42, as indicated in Fig. 4(c). We note that the QDR structures are similar to the GaSb clusters defined in Fig. 1(e). Variations in the Sb composition amongst the WLs, QDs, and QDRs are likely due to differences in their formation mechanisms. In particular, the lower Sb composition within the QDRs in comparison to that of the QDs might be due to strain relief via Sb out-diffusion, as suggested by earlier reports.[7,9,25,26] Furthermore, the lower composition in the WL in comparison to that of the 3D nanostructures may be due to Sb adatoms that cluster together during growth but then disintegrate if the critical thickness for QD formation is not reached.[27]

We now discuss the influence of QD morphology on PL emissions. Fig. 5 shows contour plots of x_{Sb} within a (a) GaSb QD and (b) GaSb QDR, along with (c) PL spectra for 2DLs (orange) and 2DLs+3DNSs (blue) normalized to the GaAs peak at 1.48 eV. For both cases, PL emissions at 1.33 and 1.48 eV are attributed to the WLs and the GaAs donor-acceptor transition, respectively. A similar trend is observed for the computed values of the WL transition energy (1.29 eV) and the GaAs bandgap energy (1.52 eV), as described in supplementary materials. Broadening of the WL peak in 2DLs likely arises from the local variations in the Sb composition, as presented in Figs. 3(b)-(d).

For the 2DLs + 3DNSs, additional PL emissions are observed at 1.08 and 1.20 eV. We note from XSTEM that most (~64%) of the nanostructures are QDs, with average height = 7nm and maximum $x_{Sb} = 0.90$, and the remainder are QDRs/clusters with lower average height 4nm and lower maximum $x_{Sb} = 0.48$. Since the effective band gap of GaAs is inversely proportional to x_{Sb} and emission energies are inversely proportional to QD size,[28] we tentatively attribute the 1.20 and 1.08 eV emissions to QDRs/clusters and QDs, respectively. Schrödinger-Poisson calculations reveal hole confinement energies of 0.34 and 0.60 eV, corresponding to 1.18 and 0.92 eV transition energies for the QDRs and QDs. Similar trends for the computed transition energies and measured PL energies confirm our assignment of the QDR/clusters and QD emissions. Since the energy difference between the ground and excited states are important for light-emitting device and solar cell applications, we report the calculated excited state energies in the supplementary materials. Furthermore, the diminished intensity of the WL emission for 2DLs+3DNSs is likely due to preferential carrier confinement within the 3D nanostructures. Similar intensities of the QDR and QD emissions suggest non-preferential carrier confinement within both nanostructure types.

In summary, we have examined the influence of QD morphology on the optical properties of GaAsSb/GaAs multilayers. We used the nanostructure sizes from STEM and local Sb composition from LEAP tomography as input into Schrödinger-Poisson simulations of confinement energies for QDs, QD-rings, and 2D layers. Due to the similar trends in computed transition energies and measured PL emission energies, we associate the emissions, in order of increasing energy, to QDs, QDRs, and 2D layers. This work opens up opportunities for tailoring PL emission energies for near to far-infrared optoelectronics by varying the QD morphology.

Supplementary Material and Data Availability

Details of growth conditions, LEAP characterization, and Schrödinger-Poisson models for GaSb/GaAs multilayers presented in the work are found in the supplementary materials section.[Error! Bookmark not defined.] The data that support the findings of this study are available from the corresponding author upon reasonable request.

Acknowledgements

This work was supported by the National Science Foundation (NSF) through the Graduate Research Fellowship Program (DGE 1256260) and (Grant No. ECCS-1610362). We also acknowledge the assistance of the staff at the Michigan Center for Materials Characterization. The data that support the findings of this study are available from the corresponding author upon reasonable request.

Figure captions

Fig. 1: Cross-sectional scanning transmission electron micrographs of GaSb/GaAs multilayers containing (a) two-dimensional layers (2DLs) and (b) GaSb 2D layers with 3D nanostructures (2DLs+3DNSs), with arrows depicting possible locations of Sb out-diffusion. Close-up views for the nanostructures are also shown: (c) GaSb QD, (d) GaSb QR/QDR, and (e) GaSb cluster/QDR.

Fig. 2: Three-dimensional reconstructions of local-electrode atom probe (LEAP) data from GaSb/GaAs multi-layers containing (a) two-dimensional layers (2DLs) and (b) GaSb 2D layers with 3D nanostructures (2DLs+3DNSs). Within the LEAP reconstructions, Sb, Ga, and As atoms are shown in blue, red, and yellow, respectively. 1D profiles of the Sb compositions within the reconstructed volume, x_{Sb}, are shown to the left of each 3D reconstruction.

Fig. 3: Local electrode atom probe iso-surfaces for GaSb/GaAs two-dimensional layers (2DLS): Sb iso-surface for (a) the entire conical specimen with $x_{Sb} > 0.20$ and x-y views of the top layer with (b) $x_{Sb} > 0.04$, (c) $x_{Sb} > 0.08$, (d) $x_{Sb} > 0.10$, and (e) $x_{Sb} > 0.16$. Lateral variations of x_{Sb} are apparent within GaAsSb 2DLs.

Fig. 4: Local electrode atom probe iso-surfaces for two-dimensional layers with three-dimensional nanostructures (2DLS+3DNSs): Sb iso-surface for (a) the entire conical specimen with $x_{Sb} > 0.24$ and x-y views of (b) the top layer with $x_{Sb} > 0.24$, and (c) the bottom layer with $x_{Sb} > 0.28$ for the 2DLs+3DNSs. Increasing the x_{Sb} of the iso-surfaces of the bottom layer reveal that the quantum rings consists of circular arrangements of quantum dots with Sb-rich cores, termed quantum dot rings.

Fig. 5: Comparison of quantum dot (QD) morphologies with photoluminescence (PL) emissions: contour plots of the fraction of Sb atoms within the reconstructed volume, x_{Sb}, for (a) a GaSb QD and (b) a quantum dot ring (QDR), with colors ranging from blue to red for low to high values.

(c) Normalized photoluminescence spectra collected at 20K from 2DLs (in blue) and 2DLs+3DNSs (in orange). Features at 1.48 eV and 1.33 eV are associated with GaAs donor-acceptor and the GaSb wetting layers transitions, respectively. Features at 1.2 and 1.08 eV are associated with emissions from the QDRs/clusters and QDs, respectively. Similar trends are computed for the transition energies of the QDs (0.92 eV), QDRs (1.18 eV), and WLs (1.29 eV), as well as for the GaAs bandgap energy (1.52 eV).

176 **Figure 1**

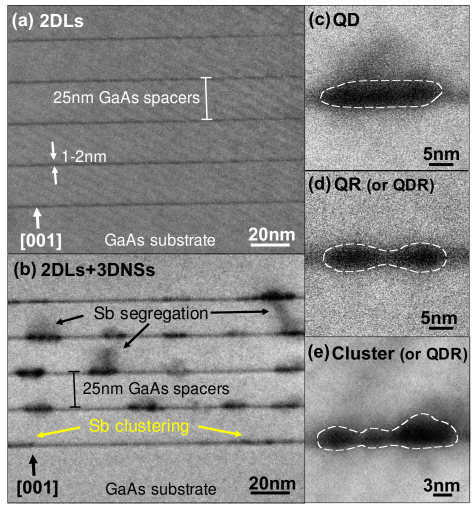

177

Figure 2

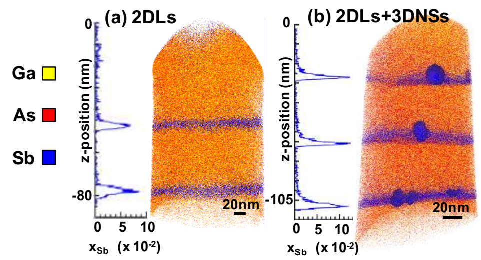
(a) 2DLs
(b) 2DLs+3DNSs
Ga
As
Sb
z-position (nm)
0
-80
-105
20nm
0 5 10
x_{Sb} (x 10^{-2})

180 **Figure 3**

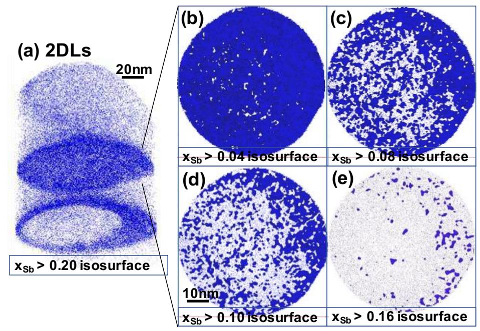

181

Figure 4

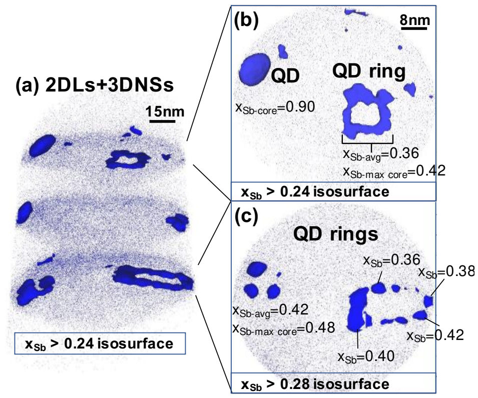
(a) 2DLs+3DNSs
15nm
x_{Sb} > 0.24 isosurface
(b)
8nm
QD
QD ring
$x_{Sb\text{-}core}$=0.90
$x_{Sb\text{-}avg}$=0.36
$x_{Sb\text{-}max\ core}$=0.42
x_{Sb} > 0.24 isosurface
(c)
QD rings
x_{Sb}=0.36
x_{Sb}=0.38
$x_{Sb\text{-}avg}$=0.42
$x_{Sb\text{-}max\ core}$=0.48
x_{Sb}=0.42
x_{Sb}=0.40
x_{Sb} > 0.28 isosurface

184 **Figure 5**

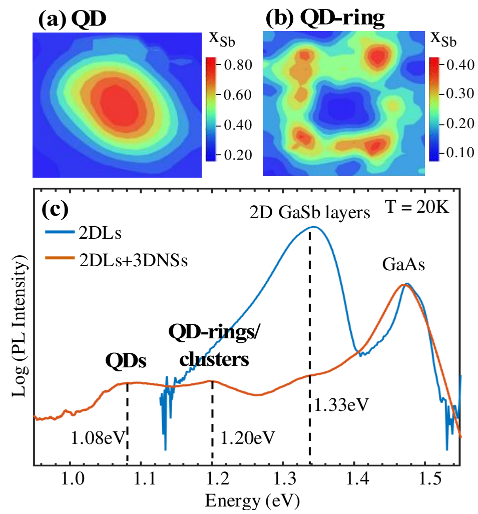

185

References

[1]M. Hayne, J. Maes, S. Bersier, V. V. Moshchalkov, A. Schliwa, L. Müller-Kirsch, C. Kapteyn, R. Heitz, and D. Bimberg, Appl. Phys. Lett. **82**, 4355 (2003).

[2]Y. Shoji, R. Tamaki, and Y. Okada, AIP Adv. **7**, 65305 (2017).

[3]W.H. Lin, C.C. Tseng, K.P. Chao, S.C. Mai, S.Y. Kung, S.Y. Wu, S.Y. Lin, and M.C. Wu, IEEE Photonics Technol. Lett. **23**, 106 (2011).

[4]M. Geller, C. Kapteyn, L. Müller-Kirsch, R. Heitz, and D. Bimberg, Appl. Phys. Lett. **82**, 2706 (2003).

[5]M. Hayne, R.J. Young, E.P. Smakman, T. Nowozin, P. Hodgson, J.K. Garleff, P. Rambabu, P.M. Koenraad, A. Marent, L. Bonato, A. Schliwa, and D. Bimberg, J. Phys. D. **46**, 264001 (2013).

[6]S.-Y. Lin, C.-C. Tseng, W.-H. Lin, S.-C. Mai, S.-Y. Wu, S.-H. Chen, and J.-I. Chyi, Appl. Phys. Lett. **96**, 123503 (2010).

[7]R. Timm, A. Lenz, H. Eisele, L. Ivanova, M. Dähne, G. Balakrishnan, D.L. Huffaker, I. Farrer, and D.A. Ritchie, J. Vac. Sci. Technol. B **26**, 1492 (2008).

[8]A.J. Martin, J. Hwang, E.A. Marquis, E. Smakman, T.W. Saucer, G. V. Rodriguez, A.H. Hunter, V. Sih, P.M. Koenraad, J.D. Phillips, and J. Millunchick, Appl. Phys. Lett. **102**, 113103 (2013).

[9]E.P. Smakman, J.K. Garleff, R.J. Young, M. Hayne, P. Rambabu, and P.M. Koenraad, Appl. Phys. Lett. **100**, 142116 (2012).

[10]J. Tatebayashi, A. Khoshakhlagh, S.H. Huang, L.R. Dawson, G. Balakrishnan, and D.L. Huffaker, Appl. Phys. Lett. **89**, 203116 (2006).

[11]M.A. Kamarudin, M. Hayne, Q.D. Zhuang, O. Kolosov, T. Nuytten, V. V. Moshchalkov, and F. Dinelli, J. Phys. D. **43**, 065402 (2010).

[12]Motlan, K.S.A. Butcher, E.M. Goldys, and T.L. Tansley, Mater. Chem. Phys. **81**, 8 (2003).

[13]C. Tseng, S. Mai, W. Lin, S.-Y. Wu, B.-Y. Yu, S.-H. Chen, S.-Y. Lin, J.-J. Shyue, and M.-C. Wu, IEEE J. Quantum Electron. **47**, 335 (2011).

[14]A.J. Martin, T.W. Saucer, K. Sun, S. Joo Kim, G. Ran, G. V. Rodriguez, X. Pan, V. Sih, and J. Millunchick, Vac. Sci. Technol. B **30**, 02B112 (2012).

[15]M. DeJarld, L. Yan, M. Luengo-Kovac, V. Sih, and J. Millunchick, J. Appl. Phys. **121**, 034301 (2017).

[16]R.J. Young, E.P. Smakman, A.M. Sanchez, P. Hodgson, P.M. Koenraad, and M. Hayne, Appl. Phys. Lett. **100**, 082104 (2012).

[17]P.J. Carrington, R.J. Young, P.D. Hodgson, A.M. Sanchez, M. Hayne, and A. Krier, Cryst. Growth Des. **13**, 1226 (2013).

[18]M.A. Kamarudin, M. Hayne, R.J. Young, Q.D. Zhuang, T. Ben, and S.I. Molina, Phys. Rev. B **83**, 115311 (2011).

[19]M. Kunrugsa, S. Panyakeow, S. Ratanathammaphan J. Crys. Growth. **416**, 73, (2015).

[20]N. Fernández-Delgado, M. Herrera, M.F. Chisholm, M.A. Kamarudin, Q.D. Zhuang, M. Hayne, and S.I. Molina, J. Mater. Sci. **51**, 7691 (2016).

[21]A.M. Beltrán, E.A. Marquis, A.G. Taboada, J.M. Ripalda, J.M. García, and S.I. Molina, Ultramicroscopy **111**, 1073 (2011).

[22]S. Birner, S. Hackenbuchner, M. Sabathil, G. Zangler, J. A. Majewski, T. Andlauer, T. Zibold, R. Morschl, A. Trellakis, and P. Vogl, Acta Phys. Pol. A **110**, 111 (2006).

[23]J. Tersoff, C. Teichert, and M. G. Lagally, Phys. Rev. Lett. **76**, 1675 (1996).

[24]R. Blossey and A. Lorke, Phys. Rev. E **65**, 21603 (2002).

[25]A. Lorke, R.J. Luyken, J.M. Garcia, and P.M. Petroff. Jpn. J. Appl. Phys. **40**, 1857 (2001).

[26]S. Kobayashi, C. Jiang, T. Takuya, and H. Sakai. Jpn. J. Appl. Phys. **43**, 662, (2004).

[27]B.R. Bennett, P.M. Thibado, M.E. Twigg, E.R. Glaser, R. Magno, B. V. Shanabrook, and L.J. Whitman, J. Vac. Sci. Technol. B Microelectron. Nanom. Struct. **14**, 2195 (1996).

[28]N.N. Ledentsov, J. Böhrer, M. Beer, F. Heinrichsdorff, M. Grundmann, D. Bimberg, S. V. Ivanov, B.Y. Meltser, S. V. Shaposhnikov, I.N. Yassievich, N.N. Faleev, P.S. Kop'Ev, and Z.I. Alferov. Appl. Phys. Lett. **67**, 656 (1995).

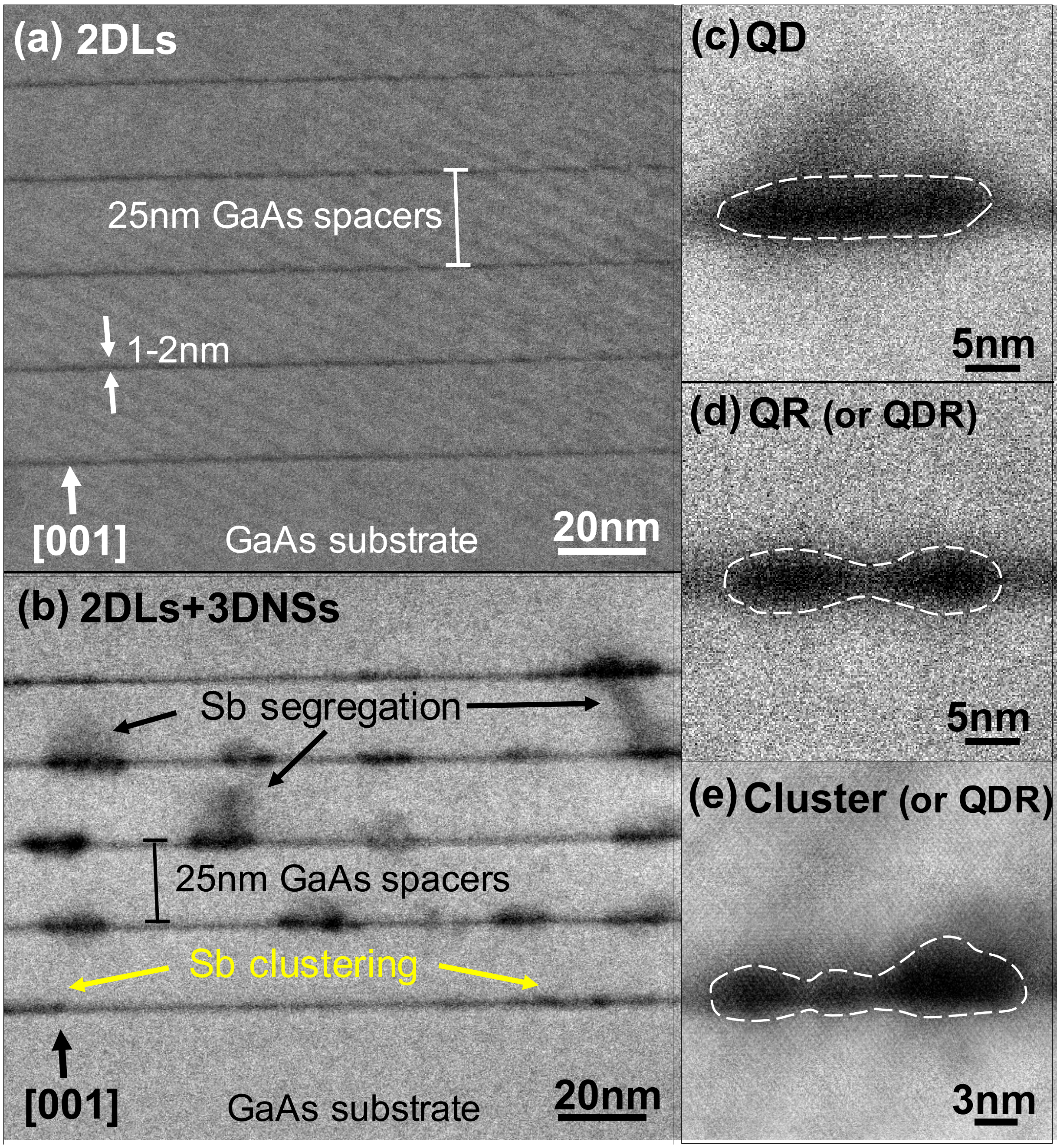
(a) 2DLs
25nm GaAs spacers
1-2nm
[001]
GaAs substrate
20nm
(b) 2DLs+3DNSs
Sb segregation
25nm GaAs spacers
Sb clustering
[001]
GaAs substrate
20nm
(c) QD
5nm
(d) QR (or QDR)
5nm
(e) Cluster (or QDR)
3nm

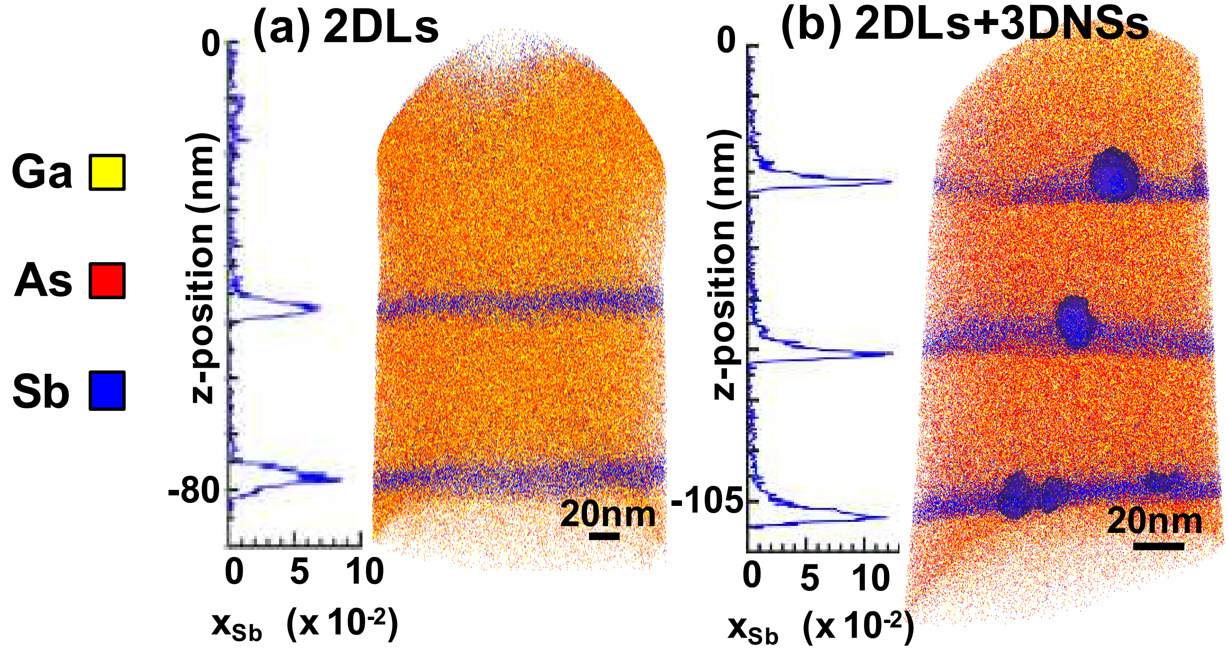
Ga
As
Sb
(a) 2DLs
0
-80
z-position (nm)
0 5 10
x_{Sb} (x 10^{-2})
20nm
(b) 2DLs+3DNSs
0
-105
z-position (nm)
0 5 10
x_{Sb} (x 10^{-2})
20nm

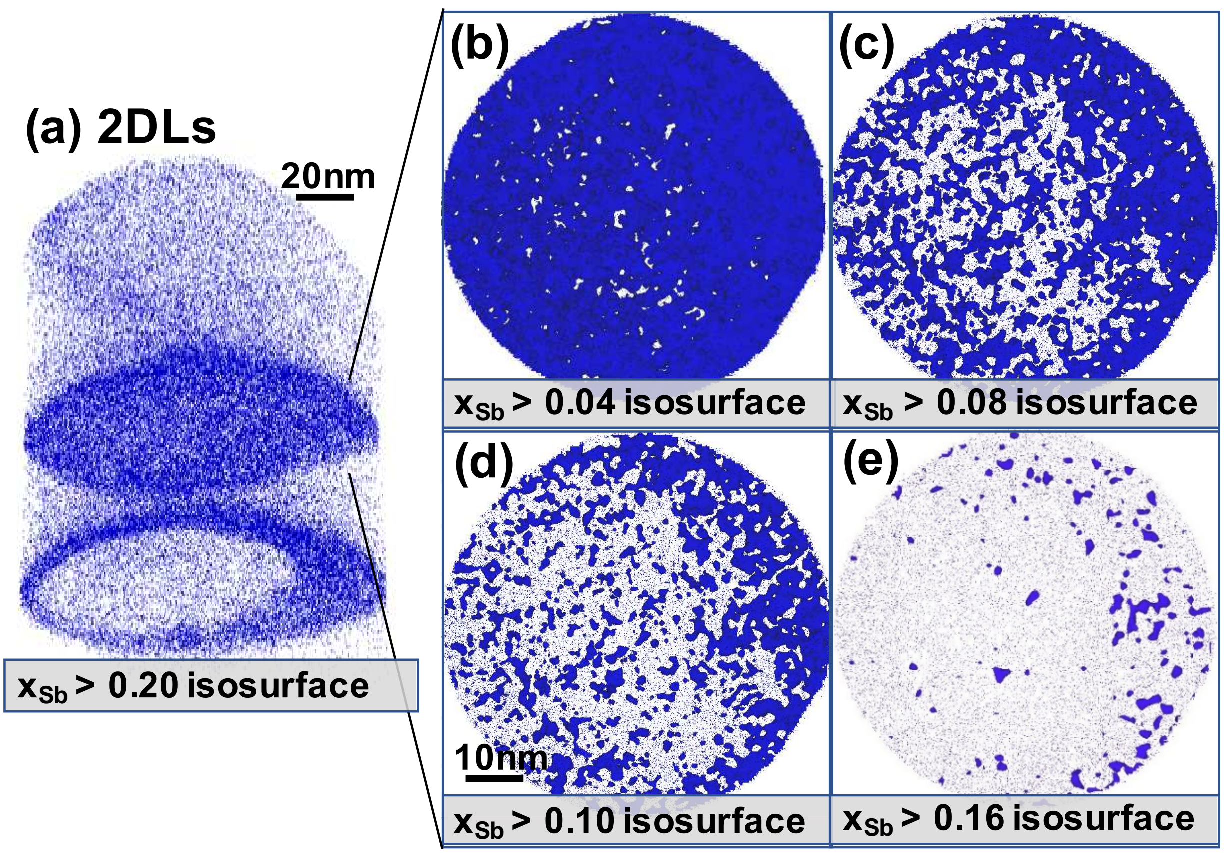
(a) 2DLs
20nm
x_{Sb} > 0.20 isosurface
(b)
x_{Sb} > 0.04 isosurface
(c)
x_{Sb} > 0.08 isosurface
(d)
10nm
x_{Sb} > 0.10 isosurface
(e)
x_{Sb} > 0.16 isosurface

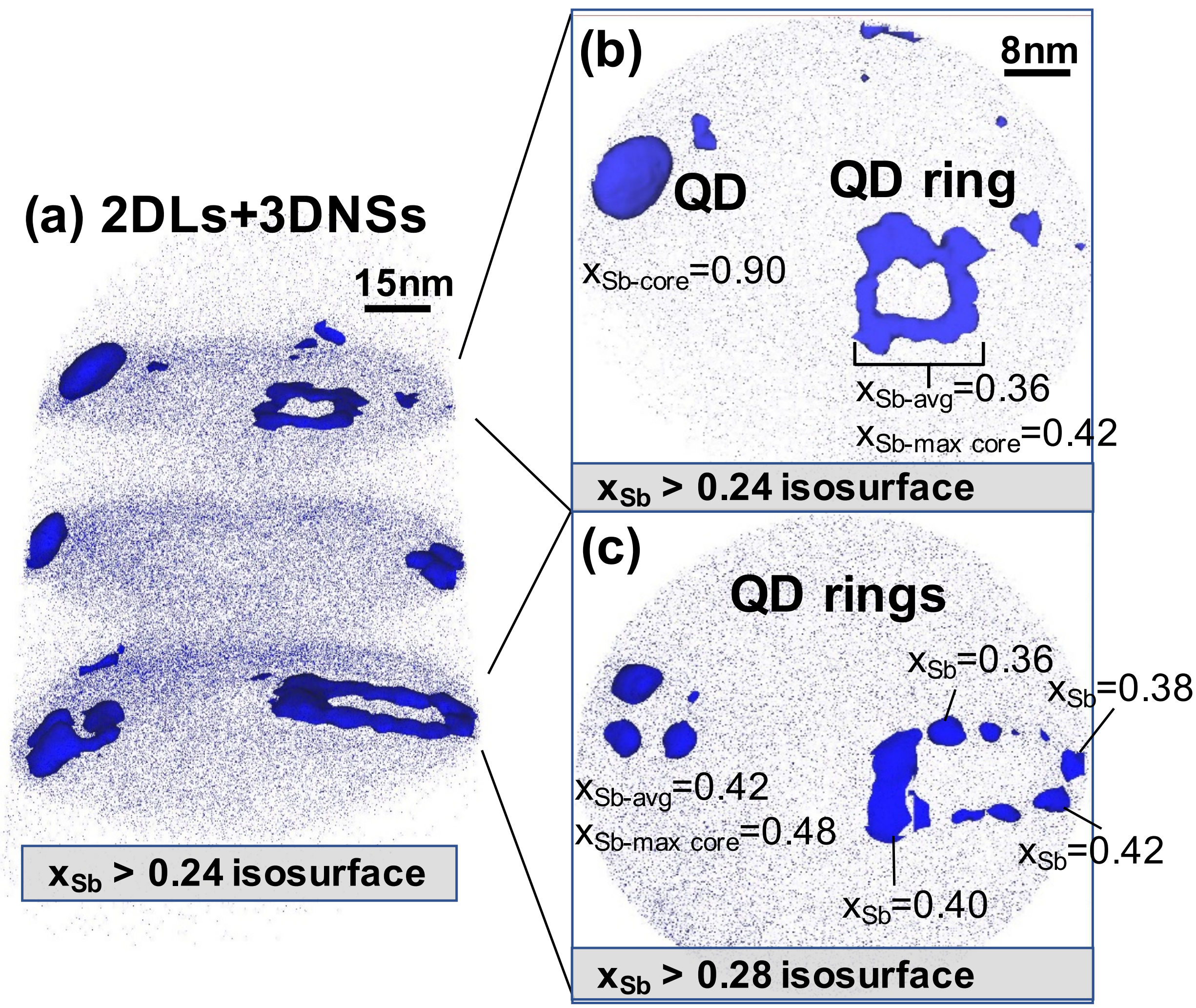
(a) 2DLs+3DNSs
15nm
x_{Sb} > 0.24 isosurface
(b)
8nm
QD
QD ring
$x_{Sb\text{-}core}$=0.90
$x_{Sb\text{-}avg}$=0.36
$x_{Sb\text{-}max\ core}$=0.42
x_{Sb} > 0.24 isosurface
(c)
QD rings
x_{Sb}=0.36
x_{Sb}=0.38
$x_{Sb\text{-}avg}$=0.42
$x_{Sb\text{-}max\ core}$=0.48
x_{Sb}=0.42
x_{Sb}=0.40
x_{Sb} > 0.28 isosurface

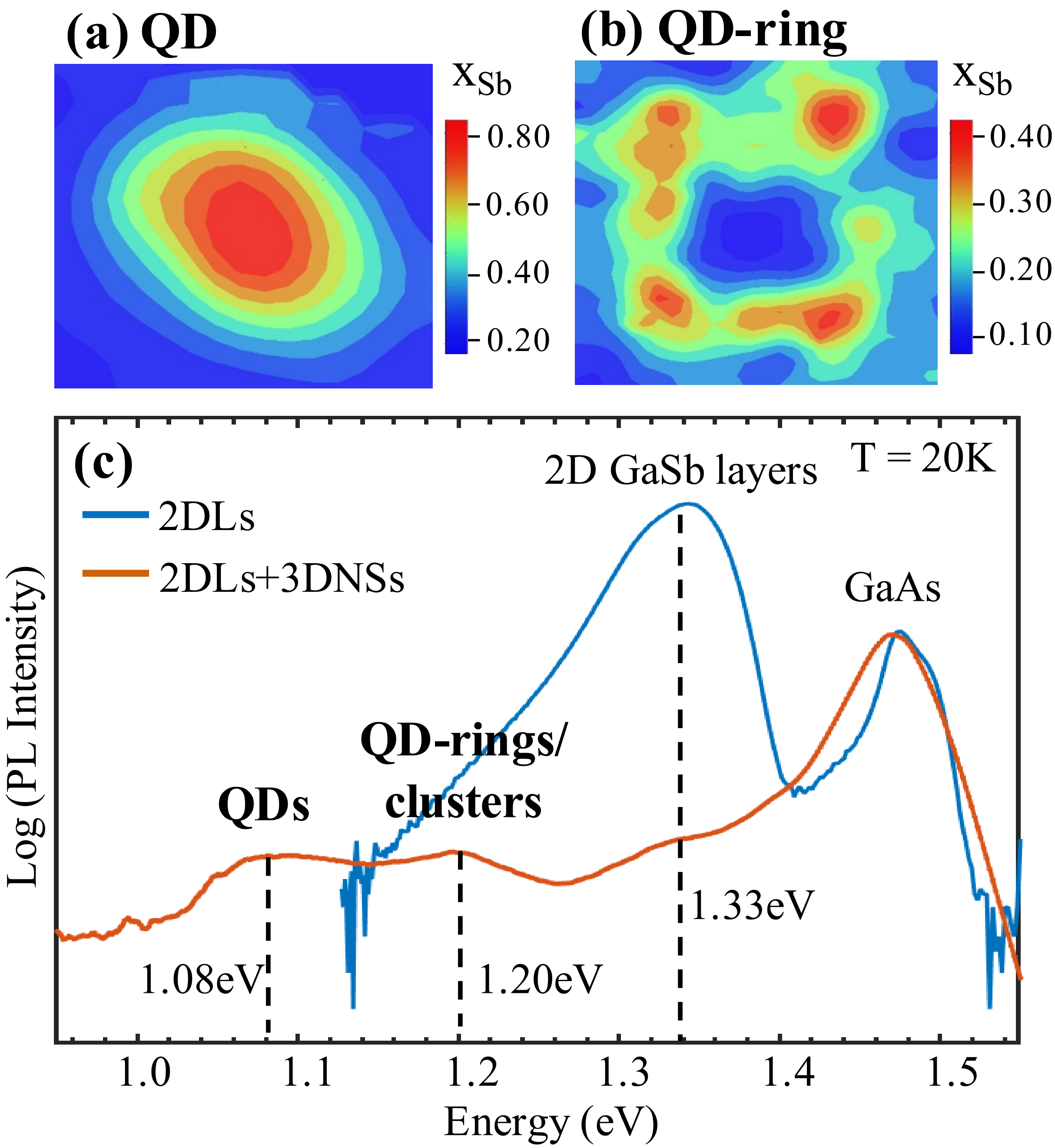
(a) QD
x_{Sb}
0.80
0.60
0.40
0.20
(b) QD-ring
x_{Sb}
0.40
0.30
0.20
0.10
(c)
T = 20K
2DLs
2DLs+3DNSs
2D GaSb layers
GaAs
QD-rings/ clusters
QDs
1.08eV
1.20eV
1.33eV
Log (PL Intensity)
1.0
1.1
1.2
1.3
1.4
1.5
Energy (eV)